Atmospheric
Chemistry
and Physics

Supplement of

Measurement report: Surface exchange fluxes of HONO during the growth process of paddy fields in the Huaihe River Basin, China

Fanhao Meng et al.

Correspondence to: Min Qin (mqin@aiofm.ac.cn)

Text S1 Meteorological and micrometeorological measurements

The meteorological data including wind speed, wind direction, air temperature, and relative humidity were recorded by an automatic weather station (HydroMetTM, Vaisala, Finland). Precipitation and solar radiation were measured with a TR-YL rain gauge (Veinasa, China) and baseline surface radiation station (BSRN3000, TRUWEL Instrument Inc., China). Soil parameters including soil temperature (TMC6-HC, ONSET, USA) and soil water content (S-SMD-M005, ONSET, USA) were measured at a depth of 5 cm. The photolysis frequencies of HONO (J(HONO)) and NO_2 ($J(NO_2)$) were calculated from global radiation (G) according to Trebs et al. (2009). The relative uncertainty of $J(NO_2)$ is > 40 % for G < 100 W m^{-2}, 10 %–40 % for G = 100–500 W m^{-2} and ≤ 10 % for G > 500 W m^{-2}. The Tropospheric Ultraviolet and Visible (TUV) radiation model was also used to calculate UV spectral irradiance and photolysis frequency for cloudless days, and the simulated photolysis frequency ($J(O^1D)$) was corrected by adopting the observed UV intensity (Liu et al., 2019a). The particle matter concentration and aerosol size distribution of 0.25–32 μm were measured using a particulate analyzer (EDM180, Grimm, Germany).

Eddy covariance measurements were performed with an integrated 3-D ultrasonic anemometer and open-path CO_2/H_2O analyzer (IRGASON, Campbell Sci. Inc., USA) mounted at 4 m height, with data collected and recorded at 10 Hz. The friction velocity (u_*) and the Obukhov length (L) were calculated with Edire software (Robert Clement, University of Edinburgh, UK). The footprint analysis was performed with the ART Footprint Tool described by (Neftel et al., 2008), which indicated that >82 % of the field was in the mast footprint on average.

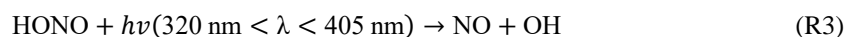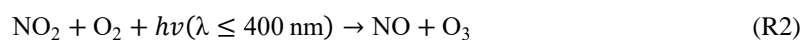**Text S2 Chemical reactions in the turbulent transport**

The chemical reactions for reactive trace gases (HONO, NO, and NO_2) need to be considered in determining HONO, NO, and NO_2 fluxes since the AG method is strictly valid only for non-reactive trace gases. The comparison of turbulent transport and chemical reaction timescales demonstrated whether chemical reactions could occur in the transport of chemical species, and thus whether these can be regarded as passive scalar (Stella et al., 2012). The ratio of turbulent transport timescale (τ_{trans}) and chemical reaction timescale (τ_{chem}) is defined as Damköhler number (DA) ($DA = \tau_{trans}/\tau_{chem}$), which identifies flux divergence from the chemical reactions (Laufs et al., 2017; Meng et al., 2022; Stella et al., 2012). The turbulent transport time was estimated between the reference height (z_{ref}) and

the ground surface (or canopy exchange height), which was simply expressed as the product of transfer

resistance and layer height (Garland, 1997):

$$\tau_{\text{trans}} = R_a(z) \cdot (z_{\text{ref}} - d - z_0) + R_b \cdot (z_0 - z_{0'})$$

$$\approx R_a(z) \cdot (z_{\text{ref}} - d - z_0) \tag{S1}$$

$$R_a(z) = \frac{u(z)}{u_*^2} - \frac{\Psi_H(z/L) - \Psi_M(z/L)}{\kappa u_*} \tag{S2}$$

where $R_a(z)$ and R_b are the aerodynamic resistance and quasi-laminar boundary layer resistance, where

R_b was small and could be neglected; z_0 and $z_{0'}$ are the roughness height for the momentum and the

scalar, respectively; Ψ_M is integrated stablity corection fuction for momentum (Sutton et al., 1993). The

chemical reaction time of HONO and NO-O_3-NO_2 triad gives characteristic timescale in turbulent

transport.

$$NO + O_3 \rightarrow NO_2 + O_2 \tag{R1}$$

$$NO_2 + O_2 + h\nu(\lambda \leq 400\,\text{nm}) \rightarrow NO + O_3 \tag{R2}$$

$$HONO + h\nu(320\,\text{nm} < \lambda < 405\,\text{nm}) \rightarrow NO + OH \tag{R3}$$

The reactions of NO + OH and HONO + OH, which are typically much lower than HONO photolysis

during daytime, were not considered in the calculation of HONO chemical time. The reaction (R3) for

the reaction of the NO-O_3-NO_2 triad could also be neglected (Stella et al., 2012). Thus, the chemical

reaction timescale for HONO and NO-O_3-NO_2 triad were estimated as follows:

$$\tau_{\text{chem}} = \frac{1}{J(\text{HONO})} \tag{S3}$$

$$\tau_{\text{chem}} = \frac{2}{\sqrt{J(NO_2)^2 + k^2\left(\overline{[O_3]} - \overline{[NO]}\right)^2 + 2J(NO_2)k\left(\overline{[O_3]} + \overline{[NO]} + 2\overline{[NO_2]}\right)}} \tag{S4}$$

where k is the rate coefficient (Walton et al., 1997), $\overline{[NO]}$, $\overline{[NO_2]}$ and $\overline{[O_3]}$ are the mixing ratios at the

measurement height. The daytime transfer time was typically less than 1 min, which was much smaller

than the HONO chemical lifetime ($\tau_{\text{chem}} \geq 9$ min). The influence of photolytic loss to overall HONO

flux was always below 10 % ($DA < 0.1$), which gave an upper limit for the flux divergence. For further

analysis, the divergence by chemical reactions could be neglected, as it does not significantly affect the

interpretation of potential HONO sources and driving forces of the HONO flux (Laufs et al., 2017). For

the NO-O_3-NO_2 triad, the chemical reactions induced a flux divergence was primarily attributed to

reaction of NO and O_3 and was limited by NO mixing ratio, which was dependent on the Damköhler

number. The DA was typically smaller than 1 in this study, while a significant increase in flux

divergence was reported when the DA exceeded 1 (Stella et al., 2012). Nevertheless, the fluxes with

chemical corrections were not available due to the lack of O_3 flux (Lenschow and Delany, 1987), which could be underestimated compared to actual fluxes. Considering the significant influence of chemical reactions on the NO and NO_2 fluxes with *DA* exceeding 1, these fluxes have been excluded from further discussion.

Text S3 Calculation of HONO sources and sinks

HONO sources

Homogeneous reaction

The HONO production from the homogeneous reaction of NO and OH is calculated as follows:

$$P_{\text{OH+NO}} = k_{\text{OH+NO}}[\text{OH}][\text{NO}] \tag{S5}$$

The rate constant of $k_{\text{OH+NO}}$ is 9.8×10^{-12} cm^3 molecules^{-1} s^{-1} (Atkinson et al., 2004), and [OH] and [NO] are the mixing ratios of OH (molecules cm^{-3}) and NO (ppbv), respectively. The OH concentrations are derived by applying the empirical equation (Liu et al., 2019a):

$$[\text{OH}] = a \times \left(J\left(\text{O}^1\text{D}\right)/10^{-5}\right)^b + c \tag{S6}$$

where *a* and *b* characterize the influence of the reactants and photolytic processes on OH, with coefficients $a = 4.2 \times 10^6$ molecules cm^{-3} and $b = 1$, respectively. The coefficient c counts light-independent OH sources, which is 1×10^6 cm^{-3} in summer.

Heterogeneous conversion of NO₂ on the surfaces

The heterogeneous conversion of NO_2 on the surface is considered as a significant source of HONO. The reaction (R4) assumes that HONO and HNO_3 are formed by equimolar disproportionation of two NO_2 molecules and immediately release HONO (Finlayson-Pitts et al., 2003; Finlayson-Pitts, 2009). The HONO production from the heterogeneous reaction of NO_2 on the aerosol surface and the ground surface can be calculated as follows:

$$2\text{NO}_2 + \text{H}_2\text{O} \rightarrow \text{HONO} + \text{HNO}_3 \tag{R4}$$
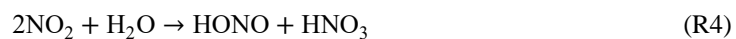
$$P_{\text{aerosol}} = \frac{v(\text{NO}_2) \times \gamma_a \times S_a \times [\text{NO}_2]}{8} \tag{S7}$$

$$P_{\text{ground}} = \frac{v(\text{NO}_2) \times \gamma_g \times [\text{NO}_2]}{8 \times MLH} \tag{S8}$$

where $v(\text{NO}_2)$ is the molecule speed of NO_2 (m s^{-1}), $v(\text{NO}_2) = \sqrt{\frac{8RT}{\pi M}}$; S_a is the aerosol surface areas (m^{-1}) derived from the aerosol size distribution, $[\text{NO}_2]$ is the NO_2 concentration (ppbv), γ_a and γ_g is the uptake coefficient of NO_2 on the aerosol surface and the ground surface, which is supposed to be 1

$\times 10^{-6}$ (Hu et al., 2023).

The vertical mixing process is determined by the turbulence, and the vertical transmission distance of HONO (Δz) over time τ could be considered as the upper limit of MLH, which can be calculated as follow (Xue et al., 2021):

$$\Delta z = \sqrt{2 \times K_z \times \tau} \tag{S9}$$

where K_z is the turbulent diffusion coefficient, with a typical value of 3×10^5 cm^2 s^{-1}, and τ is the photolytic lifetime of HONO. The calculated Δz is 205 m at 12:00, coinciding with the shortest photolytic lifetime of HONO (699 s, J(HONO) = 1.4×10^{-3} s^{-1}). Since MLH is expected to exhibit a similar variability to the boundary layer height (BLH), the diurnal profile of MLH is determined by utilizing the diurnal BLH data sourced from ECMWF (European Center for Medium-Range Weather Forecasts) and scaled by the ratio of Δz-to-BLH at 12:00, the calculated MLH is shown in Fig. S7.

Soil emission

The HONO production rate (P_{soil}) was estimated from soil HONO emission and the mixing layer height according to the following equation:

$$P_{\text{soil}} = \frac{10^9 \times 3600 \times R \times T \times F_{\text{HONO}}}{M \times P \times MLH} \tag{S10}$$

where F_{HONO} is the HONO flux (g m^{-2} s^{-1}), R is the ideal gas constant (J mol^{-1} K^{-1}), T is the temperature (K), M is the molecular weight (g mol^{-1}), P is the atmospheric pressure (Pa), MLH is mixing layer height (m).

Photosensitized conversion of NO$_2$ on the surfaces

The heterogeneous conversion of NO$_2$ on the aerosol surface and the ground surface can be parameterized as follows:

$$NO_2 + h\nu \xrightarrow{\text{surface}} HONO \tag{R5}$$
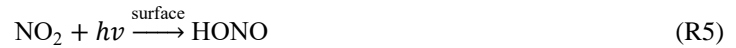
$$P_{\text{aerosol}+h\nu} = \frac{v(NO_2) \times \gamma_{a+h\nu} \times S_a \times [NO_2]}{4} \times \frac{J(NO_2)}{J(NO_2)_{\text{noon}}} \tag{S11}$$

$$P_{\text{ground}+h\nu} = \frac{v(NO_2) \times \gamma_{g+h\nu} \times [NO_2]}{4 \times MLH} \times \frac{J(NO_2)}{J(NO_2)_{\text{noon}}} \tag{S12}$$

where $\gamma_{a+h\nu}$ and $\gamma_{g+h\nu}$ are the photo-enhanced uptake coefficient of NO$_2$ on the aerosol surface and the ground surface, respectively. $\frac{J(NO_2)}{J(NO_2)_{\text{noon}}}$ is photo-enhanced factor, and $J(NO_2)_{\text{noon}}$ is set to 0.005 s^{-1} (Liu et al., 2019b; Wong et al., 2013). The photo-enhanced uptake coefficient of 10^{-6} to 10^{-4} was derived from previous studies, which is supposed to be 1×10^{-5} (Chen et al., 2023; Han et al., 2016;

Monge et al., 2010; Song et al., 2022; Wong et al., 2013).

HONO sinks

The sinks of HONO contain the photolysis (L_{photo}), the reaction of HONO with OH ($L_{\text{OH+HONO}}$) and dry deposition loss (L_{dep}), which can be calculated by the following formulas:

$$L_{\text{photo}} = J(\text{HONO})[\text{HONO}] \tag{S13}$$

$$L_{\text{OH+HONO}} = k_{\text{OH+HONO}}[\text{OH}][\text{HONO}] \tag{S14}$$

$$L_{\text{dep}} = \frac{v(\text{HONO})}{MLH}[\text{HONO}] \tag{S15}$$

where $J(\text{HONO})$ is photolysis frequency of HONO (s^{-1}), $k_{\text{OH+HONO}}$ is 6×10^{-12} cm^3 molecules^{-1} s^{-1}, which is rate constant (Atkinson et al., 2004); $v(\text{HONO})$ is deposition velocity of HONO, which is supposed to be 0.0048 m s^{-1} (Lee et al., 2016; Zhang et al., 2023).

Text S4 Calculation of OH production

The net OH production rate, $P_{\text{OH}}(\text{HONO})_{\text{net}}$, was calculated by OH production from HONO photolysis subtracting the OH loss terms (OH+HONO and OH+NO) (Eqs. (S16)). The OH production rate from O$_3$ photolysis was calculated by Eq. (S17) (Li et al., 2018; Su et al., 2008).

$$P_{\text{OH}}(\text{HONO})_{\text{net}} = J_{\text{HONO}}[\text{HONO}] - k_{\text{OH+NO}}[\text{OH}][\text{NO}] - k_{\text{OH+HONO}}[\text{OH}][\text{HONO}] \tag{S16}$$

$$P_{\text{OH}}(\text{O}_3) = 2J(\text{O}^1\text{D})[\text{O}_3]/(1 + k_3[\text{M}]/k_2[\text{H}_2\text{O}]) \tag{S17}$$

where $k_2 = 2.2 \times 10^{-10}$ cm^3 molecules^{-1} s^{-1} and $k_3 = 2.6 \times 10^{-11}$ cm^3 molecules^{-1} s^{-1} are the reaction rate constants of the O^{1}D branch reaction, respectively.
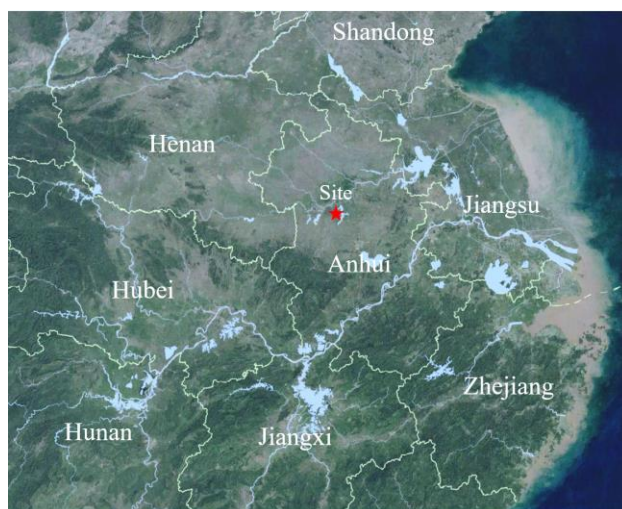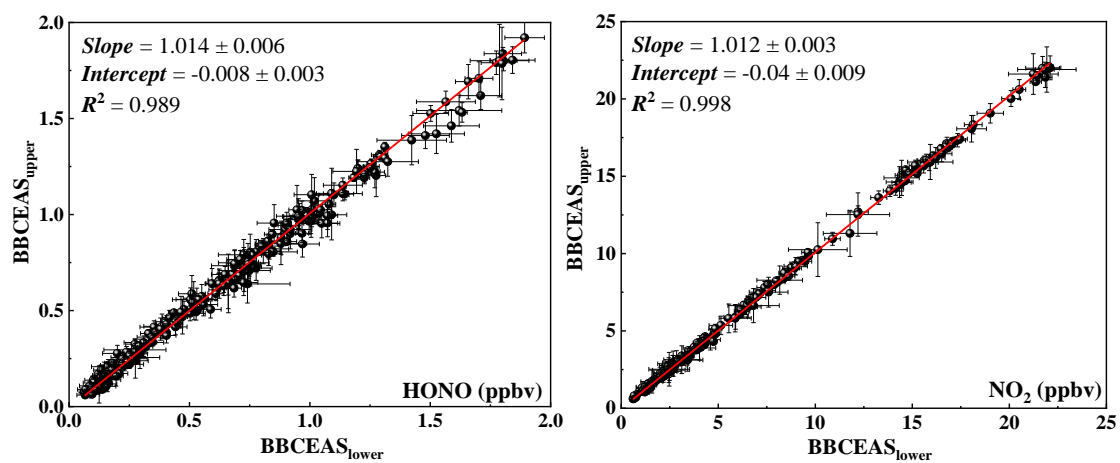
Figures

Figure S1. Location of the Shouxian National Climatological Observatory (red star, 32°25′ N, 116°47′ E). The map is adapted from ©Google Earth.
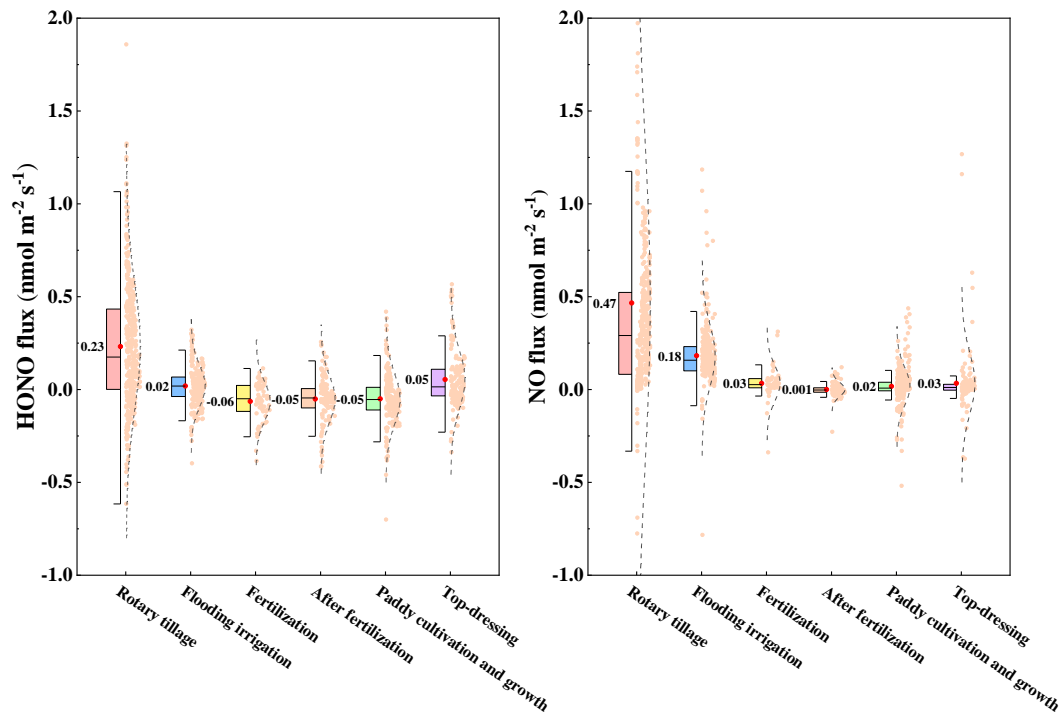

Figure S2. Intercomparison of HONO and NO_2 mixing ratios measured by $BBCEAS_{lower}$ at 0.2/0.3 m level and $BBCEAS_{upper}$ at 1.6 m level, where the slope and intercept with 2σ standard deviation are given.

Figure S3. The fluxes of HONO and NO experienced various agricultural management activities, including rotary tillage, flooding irrigation, fertilization, post-fertilization, paddy cultivation and growth, and top-dressing. The boxes represent 25 % to 75 % of data, and the whiskers are 10 %–90 % of data, while the black line and the red circle indicate the median and mean of data.
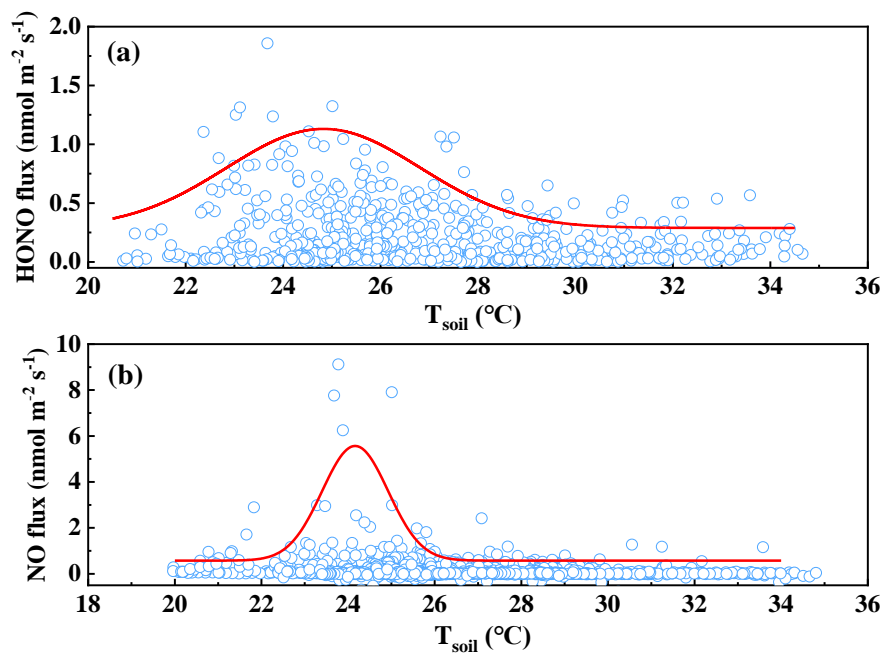

Figure S4. Emissions of (a) HONO and (b) NO as a function of soil temperature over the rotary tillage. The curves are gaussian fitting the fluxes of HONO and NO with soil temperature.
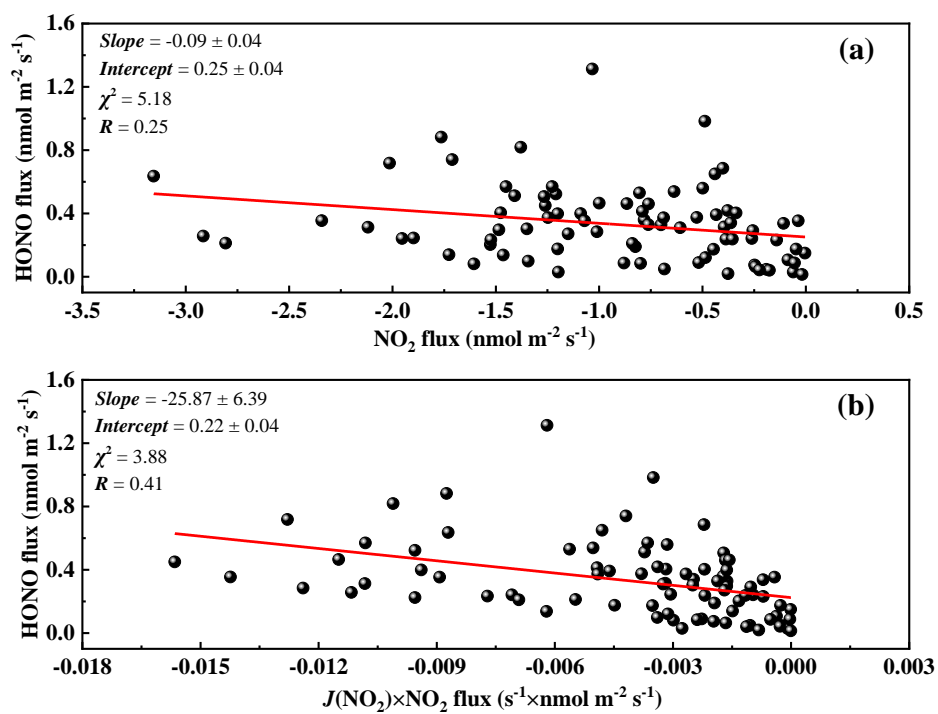
Figure S5. Correlations of the daytime HONO flux with (a) NO_2 flux and (b) the product of $J(NO_2)$ × NO_2 flux during rotary tillage.
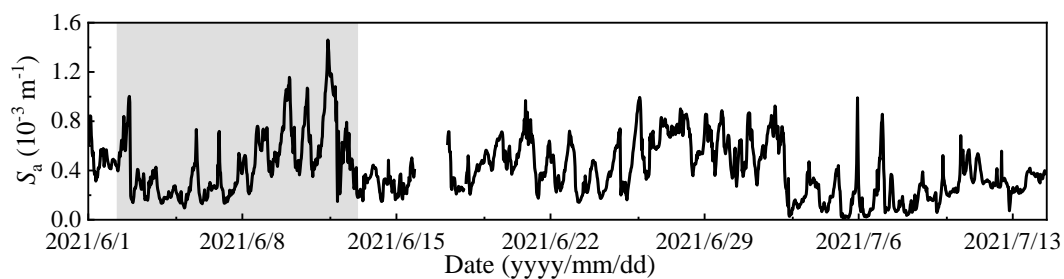

Figure S6. Time series of aerosol surface area (S_a) during the whole campaign. The shaded area represents the rotary tillage period.
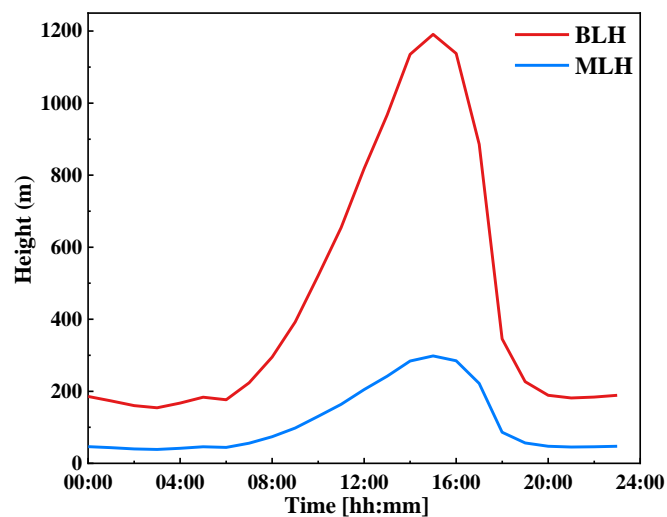
Figure S7. The diurnal variation of BLH was obtained from ECMWF and the calculated MLH.
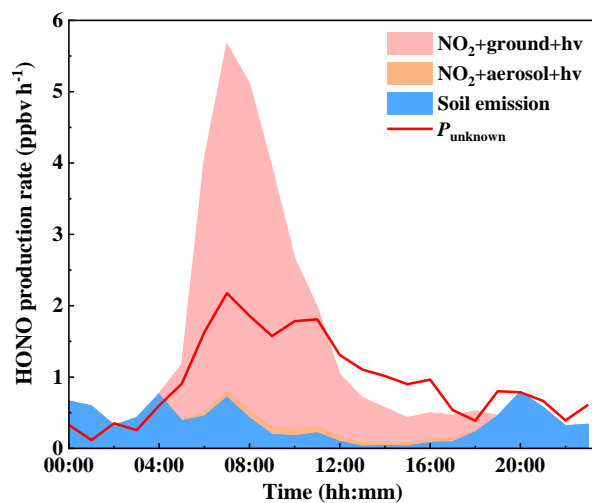

Figure S8. Diurnal variation of photosensitive conversion of NO_2 on the surfaces and HONO flux rates derived from soil emissions. The upper limit of photo-enhanced uptake coefficient of 3.5×10^{-5} was utilized to estimate the $P_{aerosol+h\nu}$ and $P_{ground+h\nu}$.
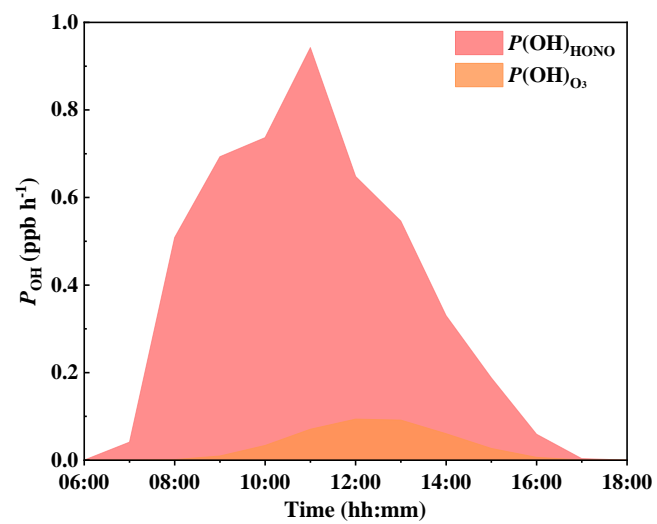
Figure S9. Diurnal variation of net OH production rate of the photolysis of HONO (P(OH)$_{HONO}$) and O$_3$ (P(OH)$_{O_3}$) over the winter campaign.

References

Atkinson, R., Baulch, D. L., Cox, R. A., Crowley, J. N., Hampson, R. F., Hynes, R. G., Jenkin, M. E., Rossi, M. J., and Troe, J.: Evaluated kinetic and photochemical data for atmospheric chemistry: Volume I -: gas phase reactions of O_x, HO_x, NO_x and SO_x species, Atmos. Chem. Phys., 4, 1461-1738, https://doi.org/10.5194/acp-4-1461-2004, 2004.

Chen, D., Zhou, L., Liu, S., Lian, C., Wang, W., Liu, H., Li, C., Liu, Y., Luo, L., Xiao, K., Chen, Y., Qiu, Y., Tan, Q., Ge, M., and Yang, F.: Primary sources of HONO vary during the daytime: Insights based on a field campaign, Sci. Total Environ., 903, 16605, https://doi.org/10.1016/j.scitotenv.2023.166605, 2023.

Finlayson-Pitts, B. J.: Reactions at surfaces in the atmosphere: integration of experiments and theory as necessary (but not necessarily sufficient) for predicting the physical chemistry of aerosols, Phys. Chem. Chem. Phys., 11, 7760-7779, https://doi.org/10.1016/10.1039/b906540g, 2009.

Finlayson-Pitts, B. J., Wingen, L. M., Sumner, A. L., Syomin, D., and Ramazan, K. A.: The heterogeneous hydrolysis of NO_2 in laboratory systems and in outdoor and indoor atmospheres: An integrated mechanism, Phys. Chem. Chem. Phys., 5, 223-242, https://doi.org/10.1039/b208564j, 2003.

Garland, J. A.: The dry deposition of sulphur dioxide to land and water surfaces, P. Roy. Soc. A-Math. Phy., 354, 245-268, https://doi.org/10.1098/rspa.1977.0066, 1997.

Han, C., Yang, W., Wu, Q., Yang, H., and Xue, X.: Heterogeneous photochemical conversion of NO_2 to HONO on the humic acid surface under simulated sunlight, Environ. Sci. Technol., 50, 5017-5023, https://doi.org/10.1021/acs.est.5b05101, 2016.

Hu, B., Chen, G., Chen, J., Xu, L., Fan, X., Hong, Y., Li, M., Lin, Z., Huang, M., Zhang, F., and Wang, H.: The effect of nitrous acid (HONO) on ozone formation during pollution episodes in southeastern China: Results from model improvement and mechanism insights, Sci. Total Environ., 891, 164477, https://doi.org/10.1016/j.scitotenv.2023.164477, 2023.

Laufs, S., Cazaunau, M., Stella, P., Kurtenbach, R., Cellier, P., Mellouki, A., Loubet, B., and Kleffmann, J.: Diurnal fluxes of HONO above a crop rotation, Atmos. Chem. Phys., 17, 6907-6923, https://doi.org/10.5194/acp-17-6907-2017, 2017.

Lee, J. D., Whalley, L. K., Heard, D. E., Stone, D., Dunmore, R. E., Hamilton, J. F., Young, D. E., Allan, J. D., Laufs, S., and Kleffmann, J.: Detailed budget analysis of HONO in central London reveals a missing daytime source, Atmos. Chem. Phys., 16, 2747-2764, 10.5194/acp-16-2747-2016, 2016.

Lenschow, D. H. and Delany, A. C.: An analytic formulation for NO and NO_2 flux profiles in the atmospheric surface layer, J. Atmos. Chem., 5, 301-309, https://doi.org/10.1007/BF00114108, 1987.

Li, D., Xue, L., Wen, L., Wang, X., Chen, T., Mellouki, A., Chen, J., and Wang, W.: Characteristics and sources of nitrous acid in an urban atmosphere of northern China: Results from 1-yr continuous observations, Atmos. Environ., 182, 296-306, https://doi.org/10.1016/j.atmosenv.2018.03.033, 2018.

Liu, Y., Nie, W., Xu, Z., Wang, T., Wang, R., Li, Y., Wang, L., Chi, X., and Ding, A.: Semi-quantitative understanding of source contribution to nitrous acid (HONO) based on 1 year of continuous observation at the SORPES station in eastern China, Atmos. Chem. Phys., 19, 13289-13308, https://doi.org/10.5194/acp-19-13289-2019, 2019a.

Liu, Y., Lu, K., Li, X., Dong, H., Tan, Z., Wang, H., Zou, Q., Wu, Y., Zeng, L., Hu, M., Min, K. E., Kecorius, S., Wiedensohler, A., and Zhang, Y.: A Comprehensive Model Test of the HONO Sources Constrained to Field Measurements at Rural North China Plain, Environ. Sci. Technol., 53, 3517-3525, https://doi.org/10.1021/acs.est.8b06367, 2019b.

Meng, F., Qin, M., Fang, W., Duan, J., Tang, K., Zhang, H., Shao, D., Liao, Z., Feng, Y., Huang, Y., Ni,

T., Xie, P., Liu, J., and Liu, W.: Measurement of HONO flux using the aerodynamic gradient method over an agricultural field in the Huaihe River Basin, China, J. Environ. Sci., 114, 297-307, https://doi.org/10.1016/j.jes.2021.09.005, 2022.

Monge, M. E., D'Anna, B., Mazri, L., Giroir-Fendler, A., Ammann, M., Donaldson, D. J., and George, C.: Light changes the atmospheric reactivity of soot, P. Natl. Acad. Sci. USA, 107, 6605-6609, https://doi.org/10.1073/pnas.0908341107, 2010.

Neftel, A., Spirig, C., and Ammann, C.: Application and test of a simple tool for operational footprint evaluations, Environ. Pollut., 152, 644-652, https://doi.org/10.1016/j.envpol.2007.06.062, 2008.

Song, Y., Zhang, Y., Xue, C., Liu, P., He, X., Li, X., and Mu, Y.: The seasonal variations and potential sources of nitrous acid (HONO) in the rural North China Plain, Environ. Pollut., 311, 119967, https://doi.org/10.1016/j.envpol.2022.119967, 2022.

Stella, P., Loubet, B., Laville, P., Lamaud, E., Cazaunau, M., Laufs, S., Bernard, F., Grosselin, B., Mascher, N., Kurtenbach, R., Mellouki, A., Kleffmann, J., and Cellier, P.: Comparison of methods for the determination of NO-O_3-NO_2 fluxes and chemical interactions over a bare soil, Atmos. Meas. Tech., 5, 1241-1257, https://doi.org/10.5194/amt-5-1241-2012, 2012.

Su, H., Cheng, Y. F., Shao, M., Gao, D. F., Yu, Z. Y., Zeng, L. M., Slanina, J., Zhang, Y. H., and Wiedensohler, A.: Nitrous acid (HONO) and its daytime sources at a rural site during the 2004 PRIDE-PRD experiment in China, J. Geophys. Res-Atmos., 113, D14312, https://doi.org/10.1029/2007JD009060, 2008.

Sutton, M. A., Fowler, D., and Moncrieff, J. B.: The exchange of atmospheric ammonia with vegetated surfaces. I: Unfertilized vegetation, Q. J. Roy. Meteor. Soc., 119, 1023-1045, https://doi.org/10.1016/S1352-2310(97)00164-7, 1993.

Trebs, I., Bohn, B., Ammann, C., Rummel, U., Blumthaler, M., Koenigstedt, R., Meixner, F. X., Fan, S., and Andreae, M. O.: Relationship between the NO_2 photolysis frequency and the solar global irradiance, Atmos. Meas. Tech., 2, 725-739, https://doi.org/10.5194/amt-2-725-2009, 2009.

Walton, S., Gallagher, M. W., and Duyzer, J. H.: Use of a detailed model to study the exchange of NO_x and O_3 above and below a deciduous canopy, Atmos. Environ., 31, 2915-2931, https://doi.org/10.1016/S1352-2310(97)00126-X, 1997.

Wong, K. W., Tsai, C., Lefer, B., Grossberg, N., and Stutz, J.: Modeling of daytime HONO vertical gradients during SHARP 2009, Atmos. Chem. Phys., 13, 3587-3601, https://doi.org/10.5194/acp-13-3587-2013, 2013.

Xue, C., Ye, C., Zhang, C., Catoire, V., Liu, P., Gu, R., Zhang, J., Ma, Z., Zhao, X., Zhang, W., Ren, Y., Krysztofiak, G., Tong, S., Xue, L., An, J., Ge, M., Mellouki, A., and Mu, Y.: Evidence for Strong HONO Emission from Fertilized Agricultural Fields and its Remarkable Impact on Regional O_3 Pollution in the Summer North China Plain, ACS Earth Space Chem., 5, 340-347, https://doi.org/10.1021/acsearthspacechem.0c00314, 2021.

Zhang, S., Li, G., Ma, N., He, Y., Zhu, S., Pan, X., Dong, W., Zhang, Y., Luo, Q., Ditas, J., Kuhn, U., Zhang, Y., Yuan, B., Wang, Z., Cheng, P., Hong, J., Tao, J., Xu, W., Kuang, Y., Wang, Q., Sun, Y., Zhou, G., Cheng, Y., and Su, H.: Exploring HONO formation and its role in driving secondary pollutants formation during winter in the North China Plain, J. Environ. Sci., 132, 83-97, https://doi.org/10.1016/j.jes.2022.09.034, 2023.